


Theoretical study of defect-mediated ionic transport in Li, Na, and K β and β'' aluminas

Suchit Negi  and Alexandra Carvalho *

*Centre for Advanced 2D Materials, National University of Singapore, 117546 Singapore
and Institute for Functional Intelligent Materials, National University of Singapore, 117544 Singapore*

A. H. Castro Neto 

*Centre for Advanced 2D Materials, National University of Singapore, 117546 Singapore;
Department of Materials Science and Engineering, National University of Singapore, 117575 Singapore
and Institute for Functional Intelligent Materials, National University of Singapore, 117544 Singapore*



(Received 22 September 2023; accepted 22 March 2024; published 11 April 2024)

Alkali-metal β/β'' aluminas are among the fastest ionic conductors, yet little is understood about the role of defects in the ion transport mechanism. Here, we use density functional theory (DFT) to investigate the crystal structures of the β and β'' phases and their vacancy and interstitial defects. We find that charge transport is likely to be dominated by alkali-metal interstitials in β aluminas and by vacancies in β'' aluminas. Lower bounds for the activation energy for diffusion are found by determining the minimum-energy paths for defect migration. The resulting migration barriers are lower than the experimental activation energies for conduction in Na β and β'' aluminas, suggesting a latent potential for optimization. The lowest activation energy of about 20 meV is predicted for correlated vacancy migration in K β'' alumina.

DOI: [10.1103/PhysRevB.109.134105](https://doi.org/10.1103/PhysRevB.109.134105)

I. INTRODUCTION

All-solid-state batteries are one of the possible solutions to address the current safety and capacity limitations of conventional batteries [1–3]. Solid-state systems are able to offer superior chemical and thermal stability compared with Li-ion batteries with traditional liquid electrolytes, which are toxic, flammable and unstable in contact with electrode materials [4]. In contrast, some solid-state electrolytes are stable in contact with metallic anodes, allowing for higher energy density storage [5]. Additionally, they can serve concurrently as ion conduction layers, electronic insulators, and as mechanical separators between the anode and the cathode, allowing for easier design and assembly [6].

The Na aluminates β alumina and β'' alumina combine high conductivity and a wide electrochemical stability window with air processability, making them exceptional materials for Na all-solid-state batteries [7]. β alumina has an ionic conductivity of $0.01\text{--}0.03\text{ S cm}^{-1}$ in single crystals at room temperature [8], of the same order of magnitude as conventional organic liquid electrolytes [9]; β'' alumina solid electrolytes, which are more difficult to grow, can have even higher ionic conductivity despite the lower crystallinity [7,8,10]. β'' alumina solid electrolytes have been employed in molten-sodium batteries as well as planar-type Na-MH batteries [11].

The β/β'' alumina solid electrolytes can also conduct Li, K, Ag, and other ions [10,12]. The measured room-temperature conductivity for Li is about one order of

magnitude lower than for Na [13]. It is generally believed that this is due to the fact that, while Na^+ ions form a plane between the spinel blocks, Li^+ ions hop between positions above and below the conduction plane, leading to slower conduction in the plane.

In contrast, the single-crystal ionic conductivity of K β'' alumina has been found to be even higher than that of the Na β'' alumina at room temperature by several groups [12,14]. Others, however, found poorer conductivity in ceramic samples, possibly due to the presence of grain boundaries and phase coexistence [15,16]. The increase of the bulk contribution to the impedance was also found to be inconsistent with previous studies [16]. Clarifying whether the ionic conductivity of K β'' alumina can achieve such high values as claimed by the earlier studies, and in what conditions, is highly desirable due to possible application of this electrolyte in K-S batteries [17], liquid metal flow batteries [18], and other devices [19,20].

The role of defects in the diffusion and conduction of cations in β and β'' aluminas has been understood since early studies [21–27]. β aluminas present a variety of stoichiometries and are often a mixture of the β and β'' alumina phases [28]. Na β alumina ideally has compositions in the ranges $\text{Na}_2\text{O} \cdot n\text{Al}_2\text{O}_3$ with $8 < n < 11$ [7]. In ideal β alumina, there is one Na atom per conduction plane per unit cell, occupying a Beevers-Ross (BR) site. However, more commonly, Na excess is present and compensated by interstitial oxygen or dopants [22,24] such as Mg^{2+} .

The resulting general formula for β/β'' aluminas is $(\text{Al}_{11-y}\text{Mg}_y\text{O}_{16})(\text{Na}_{1+x+y}\text{O}_{1+x/2})$, where the usual β alumina forms have $x + y \approx 0.25$. The excess Na is in the conduction plane occupying interstitial positions, and the predominant

*carvalho@nus.edu.sg

compensation mechanism is by interstitial oxygen defects. Different theoretical and experimental papers have suggested different structures for the cation interstitial [22,26,29–31]. Using Mg^{2+} or other dopant as a compensation agent, it is possible to further increase the occupation of the conduction plane by Na atoms until about $y \approx 0.66$ [22]. For $y \approx 0.7$, the β'' structure is stabilized instead. For such Na concentrations, not all the available Na sites of the conduction region are occupied, and the structure can be seen as containing vacancies.

Between the ideal β composition and the β'' composition, there is a continuum of nonstoichiometric structures and, for certain compositions, the defects reveal a tendency to form superstructures that have been detected by x-ray diffuse scattering [23,24]. Both Na β alumina with an excess of interstitials or Na β'' alumina with an excess of vacancies and with $y \approx 0.66$, corresponding to 1.66 Na atoms per conduction plane per unit cell, tend to form $a\sqrt{3} \times a\sqrt{3}$ superstructures [22]. The same order has been observed for cation vacancies in K β'' aluminas. However, little is known about defect ordering in other systems [24].

Given the predominance of excess Na in Na β aluminas and of Na deficiency in Na β'' aluminas, it is believed that conduction is interstitial-mediated in β aluminas and vacancy-mediated in β'' aluminas. Whittingham and Huggins [32] proposed an interstitialcy mechanism where a highly mobile interstitial cation would knock off a cation at a regular BR site, which was consistent with the correlation coefficient obtained by comparing the diffusion coefficients obtained from conductivity and from tracer diffusion in Ag β alumina.

Classical potential-energy models have been helpful in proving that the excess of Na in Na β alumina is necessary for long-range diffusion [31]. Wang *et al.* used pair-wise interaction potentials describing the long-range Coulomb interactions, short-range repulsion and polarization effects to model the interstitialcy mechanism in β aluminas, and cation vacancy mechanism in β'' aluminas, finding that correlated motion of the ions near the vacancy lead to a “nearly free” vacancy behavior in the latter [26,33]. Later, classical molecular dynamics calculations [34] were used to study the dynamics of Na in Na β'' alumina with Na deficiency, confirming the correlated motion of the Na atoms, and indicating the formation of a vacancy superlattice at low temperature, in agreement with experimental evidence. It was suggested that the stability of this superlattice depended on the distribution of Mg^{2+} dopants. Recent larger-scale molecular dynamics simulations [35] have confirmed that the interaction between the charge-carrying defects and compensating defects is detrimental to the ionic conduction.

In this study, we use density functional theory calculations to investigate the basic ion-transport mechanisms in Li, Na, and K β aluminas. We demonstrate that in β alumina interstitial mechanisms dominate, whereas in β'' -alumina vacancy mechanisms dominate, indicating that control of the occupation of the conduction plane sites is of paramount importance to increase conductivity. We suggest lower bounds for the activation energies for diffusion, indicating that both Na and K β'' aluminas have the potential to offer nearly ideal ion conduction.

II. METHODS

First-principles DFT calculations were carried out using the QUANTUM ESPRESSO package [36]. The exchange-correlation functional of Perdew, Burke, and Ernzerhof (PBE) [37] was used together with ultrasoft pseudopotentials to account for the core electrons [38]. We employed a plane-wave basis set with kinetic-energy cutoffs of 66 Ry to expand the electronic wave functions. Lattice parameters were calculated using the unit cell with a Brillouin zone sampling of $4 \times 4 \times 1$ Monkhorst-Pack (MP) grid [39]. Defect structures, formation energies, transition levels and migration barriers were calculated using $2 \times 2 \times 1$ supercells. The Brillouin zone was sampled using a Γ -centered $1 \times 1 \times 1$ MP grid [39] for all supercell calculations. Geometry optimization was performed using the Broyden-Fletcher-Goldfarb-Shanno algorithm [40] with a total-energy convergence threshold of 0.0001 Ry and a force convergence threshold of 0.001 Ry/bohr, both of which have to be simultaneously fulfilled.

We used the nudged elastic band (NEB) [41,42] method to find the minimum-energy path (MEP) on the potential-energy surface (PES). The stoppage criteria for the NEB algorithm was a norm of the force orthogonal to the path below 0.05 eV/Å. The activation energy for migration was obtained from the difference between the MEP highest saddle point energy and the absolute energy minimum. NEB calculations were performed between energy minima or between an energy minima and a saddle point derived using symmetry considerations. A total of nine images were used to construct the MEPs.

III. RESULTS AND DISCUSSION

A. Crystal structure

In this section, we describe the structures and compositions used in our models, which typify both β alumina ($8 < n < 11$) and β'' alumina ($5 < n < 7$).

1. Na and K β aluminas

The nominal phase formula of stoichiometric $X\beta$ alumina, where $X = \{\text{Li}, \text{Na}, \text{K}\}$, is $X\text{Al}_{11}\text{O}_{17}$, as determined in the seminal works of Beevers *et al.* [10,43–45]. The Na and K β aluminas were found to belong to space group 194 (D_{6h}^4) [44]. Figure 1(a) shows the Na β alumina unit cell containing two formula units (f.u.). The calculated lattice parameters can be found in Appendix A, Tables II and III and are within 0.2 Å of the experimental values.

The key features of the structure are the Na planes, also referred to as the “conduction region” which alternate with Al-O blocks, also referred to as “spinel blocks” [7,45,46] by analogy with the MgAl_2O_4 spinel structure [47]. In the spinel block, Al atoms are surrounded by oxygen octahedra or tetrahedra. This block is non-ion-conducting and remains nearly undisturbed when the alkali-metal ions move. Figure 1(b) shows the Na or K sublattices at the conduction plane. The sites occupied by Na ions are named “Beevers-Ross” (BR) sites [46]. The unoccupied but crystallographically equivalent site is named “anti Beevers-Ross” (aBR) site [14,46]. All the processes of interest to ion conduction happen in this conduction region.

TABLE I. Calculated activation energies for migration (W_{mig}) of alkali-metal vacancy and interstitial defects, and experimental activation energy derived from conductivity experiments (E_a). Values in square brackets are for a correlated two-atom migration. LT and HT refer to low temperature and high temperature, respectively. Values in *italic* were reported for single crystals. The calculated and experimental values can be directly compared if the material has pre-existing defects of either type, or in thermodynamic equilibrium if the formation energy of one of the defects is zero or negative.

Host	Prevailing defect	Calc. W_{mig}		Expt. E_a
		V_X^{\bullet}	X_i^{\bullet}	
Li β	Li_i^{\bullet}	0.27	0.17	0.24^a 0.27^b
Li β'' : Mg	V_{Li}^{\bullet}	0.33 [0.32]	0.45	0.30^c
Na β	Na_i^{\bullet}	0.30	0.09	0.15^c 0.16^a
Na β'' : Mg	V_{Na}^{\bullet}	0.03 [0.08]	0.12	$0.28\text{--}0.33^d$ (LT) $0.20\text{--}0.31^e$ (LT) 0.03^e (HT) $0.09\text{--}0.12^e$ (HT)
K β	K_i^{\bullet}	0.72	0.08	$0.28\text{--}0.56^f$
K β'' : Mg	V_{K}^{\bullet}	0.03 [0.02]	0.37	0.15^e (LT) 0.186^g 0.09^h (HT)

^aReference [13].

^bReferences [50,68].

^cReference [10].

^dReference [61].

^eReference [12].

^fReference [67].

^gReference [16].

^hReference [25].

TABLE II. Unit-cell lattice parameters and electronic band gaps of the pristine Na and K β aluminas, idealized β'' aluminas and Mg-stabilized β'' aluminas ($x = 1$). Experimental values are given in brackets.

Structure	a (Å)	c (Å)	Band gap (eV)
Na β	5.597 (5.594 ^a)	22.485 (22.53 ^a)	4.61
Na β''	5.680 (5.60 ^a)	34.059 (34.11 ^a)	1.98
Na β'' : Mg	5.698	33.784	3.58
K β	5.597 (5.61 ^b)	22.527 (22.75 ^b)	4.80
K β''	5.689 (5.595 ^a)	34.689 (34.226 ^a)	1.90
K β'' : Mg	5.704	34.421	4.21

^aReference [45].

^bReference [75].

TABLE III. Lattice parameters and electronic band gaps of Li β alumina, idealized β'' alumina, and Mg-stabilized β'' alumina ($x = 1$).

Structure	a (Å)	b (Å)	c (Å)	Bandgap (eV)
Li β	11.192	5.596	22.462	4.63
Li β''	5.683		34.354	2.09
Li β'' : Mg	5.670		34.544	3.68

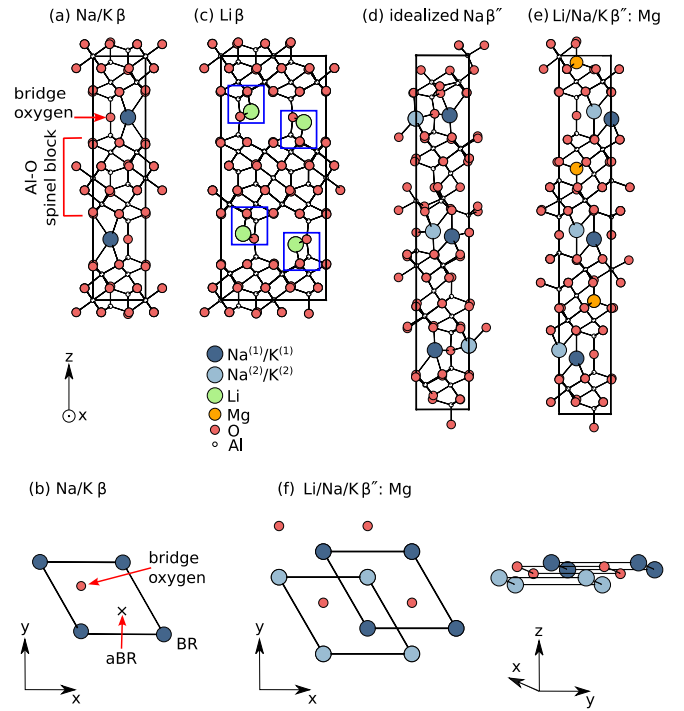


FIG. 1. Structure of β and β'' alumina crystals: (a) unit cell of Na or K β aluminas ($\text{NaAl}_{11}\text{O}_{17}$), and (b) detail of the sites in the conduction region, unit cell of (c) Li β alumina ($\text{LiAl}_{11}\text{O}_{17}$), (d) idealized β'' alumina (NaAl_5O_8), (e) Mg-stabilized β'' alumina ($\text{Na}_2\text{MgAl}_{10}\text{O}_{17}$), and (f) detail of the conduction plane of β'' alumina. The structures of the β'' aluminas are similar for all three alkali metals.

2. Li β alumina

The Li β alumina structure is similar to the Na and K β alumina structures [Fig. 1(c)]. The main difference is that the Li atoms are displaced 0.56 \AA above or below the BR sites, bonding to the neighboring oxygen atoms of the spinel layers immediately above or below, with a consequent doubling of the primitive unit cell along the \hat{x} direction. The corresponding distortion energy is 0.34 eV per unit cell. The resulting space group 18 (D_2^3), as determined with tolerances of 0.1 \AA and 0.5° for distances and angles, respectively.

Experimental evidence of the displacement of Li atoms from the BR sites can be found in the frequency of the Raman bands of the Li translational modes, found at $340\text{--}410 \text{ cm}^{-1}$, higher than expected from the corresponding values reported for other alkali-metal ions [48]. Besides, the probability of occupation of the out-of-plane position by Li can also be derived from an analysis of NMR ^7Li quadrupole interactions below 100 K [49,50]. An activation energy for out-of-plane motion of 29 meV has been determined in $93\%\text{Li}/7\%\text{Na}$ β alumina, consistent with the value 42 meV derived from our calculations [50]. Another study using neutron and x-ray diffraction in single crystals with approximately $61\%\text{Li}/39\%\text{Na}$ suggested that the Li atoms are placed 1 \AA above the BR site at low temperature [51]. The displacement is larger than predicted by our calculations and could possibly be due to the presence of the larger Na ions in the experiment. In contrast, a neutron-diffraction study in $50\%\text{Li}/50\%$ sodium β alumina

[52] determined that the Li atoms sit 1 Å above the mO site at 4.2 K, which is in conflict with our calculations where such position is found to be a saddle point, as will be discussed.

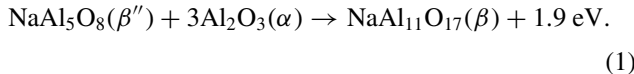
3. Idealized β'' aluminas

The key difference between β and β'' aluminas is the stacking sequence of the combined spinel and conduction double layers: in the β structure, they have AB stacking, while in the β'' structure they have ABC stacking; the experimental structure belongs to space group 166 (D_{3d}^3) [53]. The idealized phase formula of Na β'' alumina is NaAl_5O_8 , of which three f.u. make up a primitive unit cell. We have not found experimental or theoretical reports of the structure of the ideal stoichiometric β'' phase. Rather, β'' alumina is often stabilized by extrinsic divalent cations [7] such as Mg^{2+} .

Our idealized structure [Fig. 1(d)], given as Supplemental Material [54], is based on the structure of potassium β'' aluminogallate [55], where 30 Al atoms are distributed over 36 Al sites (octahedral and tetrahedral) and 48 O atoms distributed over 51 O sites. For the purpose of the DFT calculations, we have randomly chosen the positions of the Al and O atoms in the spinel block as they have little influence on ion conduction. The unit cell has twice the number of X ions per conduction plane compared with β alumina, and instead of forming a planar lattice, they are staggered 0.22 Å or 0.14 Å above or below the BR (or aBR) sites for $X = \text{Li}, \text{Na}$ and K , respectively [Fig. 1(d), Supplemental Material [54]].

The Na β'' in-plane lattice parameter is 1.6% larger than that of Na β alumina, and 1.5% larger than the experimental value (see Appendix A). The c parameter is 3.2% smaller than the experimental value [45].

Inspired by the phase diagram of the $\text{Na}_2\text{O}/\text{Al}_2\text{O}_3$ system [56], we compare the formation energy of the idealized Na β'' phase with respect to the Na β and α alumina phases, obtaining



Thus the undoped Na β'' phase is unstable (Fig. 2). Moreover in the calculated DFT band structure of idealized Na β'' is p -type doped, with the Fermi level at the valence band top, possibly due to the Al vacancies (see Appendix A). This justifies theoretically the need to dope the material with stabilizing species. These have to be taken into account in our model to reproduce the electron-insulating behavior and the right defect charge states, and will be considered in the next section.

4. Mg-stabilized β'' aluminas

Divalent cations such as Mg^{2+} act as stabilizers of the β'' phase by compensating the charge of the additional X ions without the necessity to change the spinel layer structure [7,57,58]. The ideal formula for Mg-stabilized Na β'' alumina is $\text{Na}_{1+x}\text{Mg}_x\text{Al}_{11-x}\text{O}_{17}$ [Figs. 1(e)–1(f)] where the Mg content x can be varied while keeping the number of additional Na atoms equal to the number of substitutional Mg at Al sites (Mg_{Al}) so as to keep charge neutrality. We estimate $x = 2$ with three Na atoms per unit cell and per plane to be the highest possible Na packing, with a minimum Na-Na distance of 2.9 Å, comparable to the double of the ionic radius of Na^+

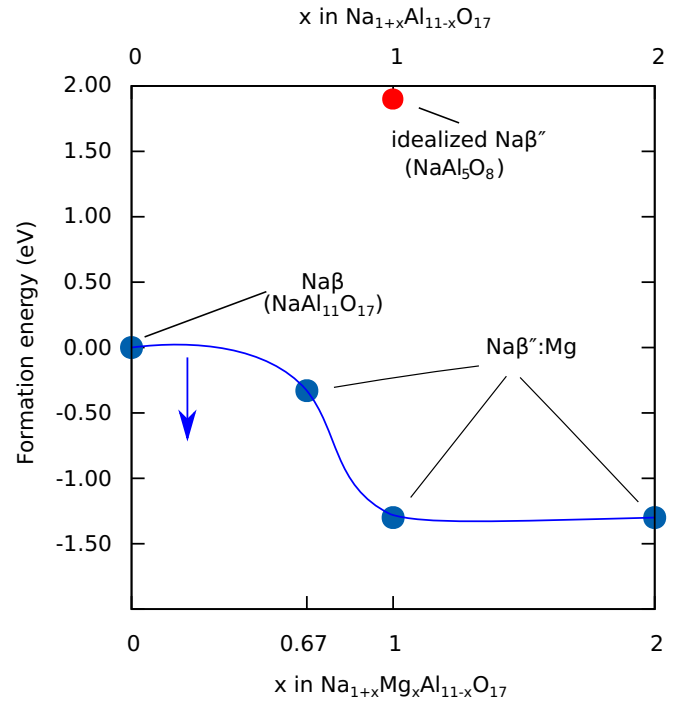
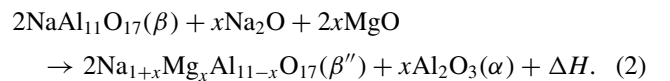


FIG. 2. Formation energies of idealized Na β'' and Mg-stabilized Na β'' phases relative to Na β alumina, from reaction (2). The blue curve corresponds to the Mg-stabilized Na β'' phase with phase formula $\text{Na}_{1+x}\text{Mg}_x\text{Al}_{11-x}\text{O}_{17}$. The special case for $x = 0$ yields β alumina. The red dot corresponds to the idealized Na β'' alumina phase (NaAl_5O_8).

(1.02 Å). Experimentally, $x \approx 0.66$ has been reported [22,46] and possibly an imbalance of Na compared with Mg due to sodium evaporation above 1600 °C [8].

We have estimated the formation energy of the Mg-doped Na β'' alumina using the equation



Adding a small fraction of Mg lowers the formation energy relative to Na β phase (Fig. 2), thus making the Mg-stabilized Na β'' phase more favorable over the Na β phase. While the formation energy of idealized Na β'' is positive, that of the Mg-stabilized Na β'' phases is now negative. Mg-stabilized Na β'' aluminas where $x = 1$ and $x = 2$ in the formula $\text{Na}_{1+x}\text{Mg}_x\text{Al}_{11-x}\text{O}_{17}$ are insulators with a clean band gap (see Appendix A, Fig. 9). Figure 1(e) shows the structure for $x = 1$, with composition $\text{Na}_2\text{O} \cdot \text{MgO} \cdot 5\text{Al}_2\text{O}_3$, of which three f.u. make up a primitive unit cell. The three Mg_{Al} are placed one in each spinel block and as far as possible from the conduction planes (see Supplemental Material [54] for an analysis of the energetics of the Mg_{Al} substitution). The resulting structure resembles that of undoped Na β'' alumina [Fig. 1(d)], with the same stacking sequence and similar up and down staggering of the Na ions in the conduction region, which occupy all the equivalent BR and aBR sites. Its optimized lattice parameters are given in Appendix A Table II. The structures of Mg-doped Li and K β'' aluminas are very similar to that of Na β'' alumina. The structure with $x = 1$

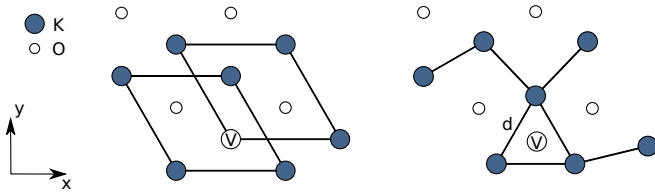


FIG. 3. Schematic representation of a vacancy in Mg-stabilized Na or K β'' alumina before relaxation (left) and after relaxation (right). “V” indicates a vacant site. Only atoms at the conduction plane are shown for clarity. d indicates the nearest-neighbor distance for the atoms at the center of the reconstructed vacancy structure.

has the same number of X ions in every conduction plane and therefore we use it as a model in subsequent calculations for all β'' aluminas, unless otherwise stated.

B. Defect structures

1. Vacancy

We created a single vacancy in one of the conduction planes, for each of the materials studied, using a $2 \times 2 \times 1$ supercell.

In the Li β alumina, the removal of the Li^+ ion leads to an expansion of the distance between its two nearest bridge oxygen neighbors in the conduction region by 18%, whereas the neighboring Li remains bonded to the respective oxygen neighbors. In the Na and K β aluminas, the vacancies retain the trigonal symmetry of the original sites, with the triangle of bridge oxygen nearest neighbors, in the same (0001) plane, contracting by 18% and 8%, respectively.

In the β'' aluminas, the distance between the V'_X nearest X neighbors (d) contracts by 2%, 54%, and 30% for $X = \text{Li}$, Na, and K, respectively. The structure of the reconstructed vacancy is shown in Fig. 3. In the resulting structure, three X atom rings form around the vacant site, and the adjacent rings of X atoms around the oxygen sites become five-atom rings instead of six-atom rings. This planar arrangement is more prominent in K, where the nearest-neighbor distance between the atoms closest to the vacancy site (d) is $\approx 4 \text{ \AA}$ compared with the K^+ ionic radii $\approx 1.38 \text{ \AA}$.

In the case of the β phases, the presence of the vacancy disturbs the positions of the Na atoms in the other conduction plane as well. In the case of the β'' phases however, the relaxation in the other conduction planes was negligible. In all cases changes to the spinel structures are negligible.

2. Interstitial

As considered in Sec. III A, the conduction planes of both β and β'' aluminas have four sites equidistant to the bridging oxygens. In β alumina, two of these are occupied by X (the BR sites), and two are unoccupied (the aBR sites)—see Fig. 4. However, in β'' alumina all four sites are occupied by X and are crystallographically equivalent. Additionally, there is another high-symmetry interstitial site named the mid-oxygen (mO) site, equidistant from an aBR site and a BR site. Lastly, we have considered split-interstitials consisting of two X atoms at adjacent mO sites, replacing the original atom at the BR site.

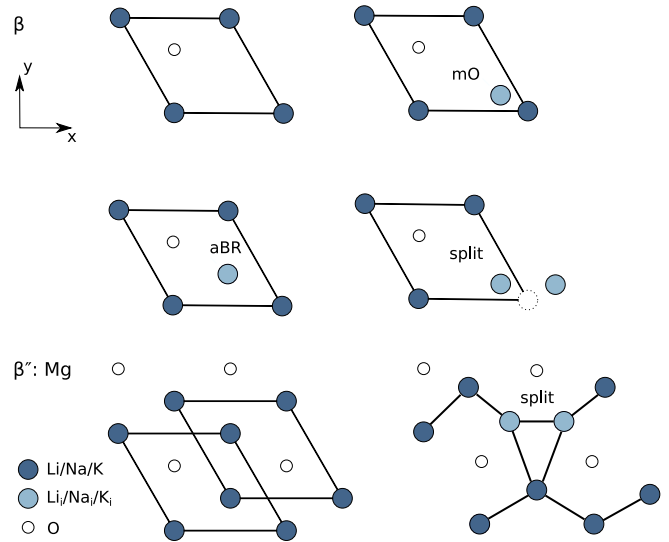


FIG. 4. Schematic representation of the interstitial sites at the conduction planes of β alumina (top) or β'' alumina (bottom). The mO and aBR sites are unstable with respect to relaxation to the split-interstitial configuration. The split-interstitial configurations are shown at the relaxed geometries obtained for Na β/β'' aluminas. Only atoms at the conduction plane are shown, where the light blue atoms represent the interstitial atoms. A dotted circle represents the BR site.

In Li β alumina, the lowest-energy configuration is a distorted $[1\bar{1}0]$ split-interstitial, with two Li atoms approximately situated between the original Li site and the aBR site. In Na β alumina, a $\langle 10\bar{1}0 \rangle$ split interstitial is the only stable configuration. Both the aBR interstitial and the mO interstitial relax to the split interstitial configuration. In K β alumina, the $\langle 10\bar{1}0 \rangle$ split-interstitial and the aBR interstitial are distinct but degenerate in energy.

Experimental studies on Na β alumina suggest Na ions start occupying the mO site in Na-rich β alumina [22,29,30]. This is consistent with the results of our calculations, since in the split-interstitial configuration, each of the Na interstitial atoms is only 0.4 \AA away from the respective nearest mO site. The relaxed geometry of the configuration is shown in Fig. 4 where the distance between the Na atoms is 3.57 \AA .

As for the Mg-stabilized Na β'' alumina, Na ions occupy all the available BR (or aBR) sites in the conduction region. Thus only the vicinity of mO interstitial sites is available for interstitial Na ions, as shown in Fig. 4. The split-interstitial, with two atoms occupying adjacent mO sites instead of the original BR or aBR site, was found to be the only stable structure. The presence of the Na interstitials has little influence on the atoms outside the conduction region.

C. Defect-formation energies

We now investigate the role of vacancy and interstitial defects in the ionic diffusion and charge conduction. If the defects are thermally generated, in equilibrium conditions, the activation energy for conduction is the sum of two terms—the energy for defect formation plus the energy for defect migration [59,60].

However, defects may be present due to processes during growth. For example, the β'' aluminas are usually Na-deficient, with the presence of Na vacancies [61], and this is believed to result from Na evaporation above 1600 °C [8]. In such material, the activation energy for conduction measured in a closed system is the migration energy only. Thus, migration energies are the minimum bound for the activation energy.

In an alkali-metal battery context, the alkali-metal chemical potential can vary across the electrolyte due to the proximity to the cathode or anode. Here, we calculate the formation energy of alkali-metal vacancies (V_X) and interstitials (X_i) in X -rich conditions, where $X = \{\text{Li, Na, K}\}$.

Even though β aluminas are wide gap insulators, we assume that its Fermi level (E_F) is well defined and take it to be the chemical potential for electrons. The defect formation energy in relative charge state q is then given by

$$E_f(D^q) = E_t(X\beta : D^q) - E_t(X\beta) \pm E_t(\text{bcc-X}) + qE_F + E_{\text{corr}}, \quad (3)$$

where $E_t(X\beta : D^q)$, $E_t(X\beta)$, and $E_t(\text{bcc-X})$ are the total energies of the supercell with the defect, the pristine supercell, and the metallic reservoir of element X , respectively, and the $-$ ($+$) signs are for interstitial (vacancy) defects. Here q specifies the effective charge of a defect relative to the neutral unperturbed lattice. In the case of the Na vacancy in Na β alumina, when only the Na^+ ion is removed, $q = -1$, and the vacancy is represented as V_{Na}' , adopting the Kröger-Vink notation [62]. Similarly, the addition of an Na^+ ion, with charge $q = 1$, is represented by Na_i^+ . In both cases, the supercell has a total charge ($q = \pm 1$),¹ a compensating jellium background with charge $-q$ is inserted to remove the divergence of the energy in a periodic supercell [63].

The correction term E_{corr} accounts for finite \mathbf{k} -point sampling, and for the spurious electrostatic interactions between supercells, including the electrostatic interaction between the defect and its periodic images, and with the neutralizing background [64,65]. We have estimated this correction for the β alumina supercell by extrapolating the dependence of a vacancy transition level energy on the in-plane supercell lattice parameter (see Supplemental Material [54]). The calculated correction is close in magnitude to the uncertainty in determining the potential alignment between defective and bulk supercells, and much smaller than the band gaps of the materials considered. Nonetheless E_{corr} has been included in the charge-dependent defect formation energies for vacancies and interstitials.

Band-filling effects can be neglected since we use the Γ point for sampling and that is the location of the direct band gap of the β and β'' aluminas [64,66].

The vacancy ($-/0$) transition level is close to the top of the valence band (E_v), indicating that vacancies are always negatively charged (V_X'). Similarly the ($0/+$) transition levels

¹For example, a pristine supercell of Na β alumina has 1152 explicit electrons, of which nine per Na atom, while a similar supercell containing a V_{Na}' defect has 1144 explicit electrons.

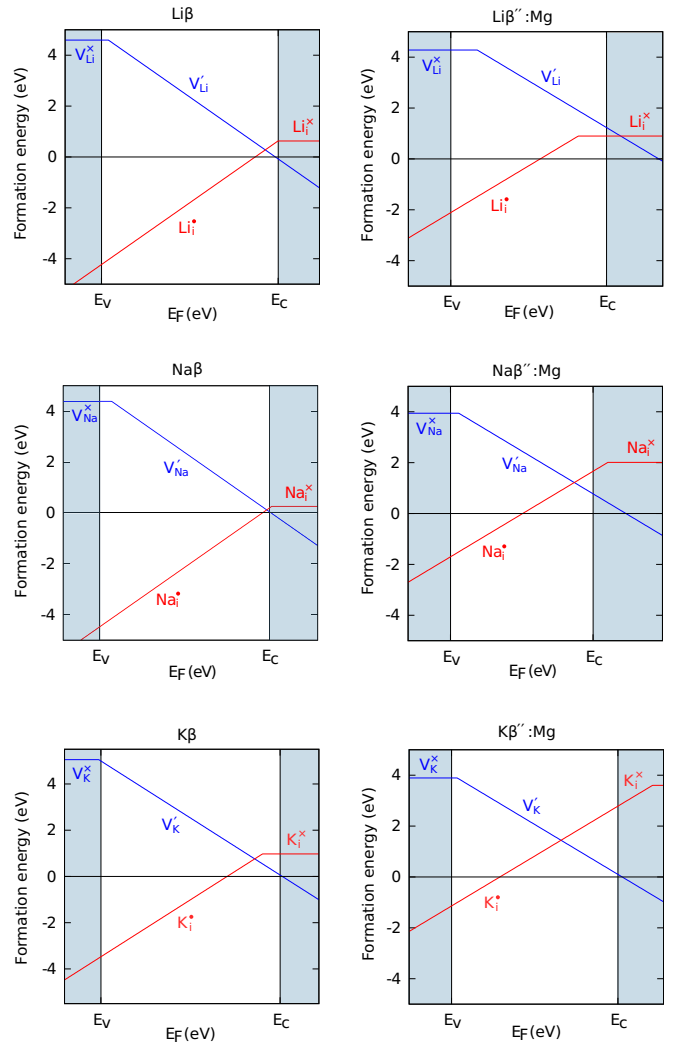


FIG. 5. Vacancy and interstitial formation energies in X -rich conditions ($X = \{\text{Li, Na, K}\}$). The formation energies for defects in the β alumina phases are shown on the left, and those in the Mg-stabilized β'' alumina phases are shown on the right. The band gap values were calculated and can be found in Appendix (Tables II and III).

of interstitial defects are close to the conduction band (E_c) indicating that interstitials are always positively charged (X_i^+). Thus both X vacancies and interstitials can in principle be responsible for ionic charge conduction.

In the case of the β aluminas, if the Fermi level is close to the conduction band, both vacancies and interstitials can be created with nearly vanishing or negative formation energy, but interstitials are more favorable over a wide range of Fermi-level energies.

In the case of the β'' aluminas, the formation energies of interstitial defects are higher than in the corresponding β aluminas, because the conduction plane is more densely packed. However, neutral vacancy formation energies are still high, around 4 eV in X -rich conditions (see Fig. 5).

The definition of the chemical potentials in X -poor conditions in battery systems depends on the electrodes used. In NaS batteries, Na-poor conditions (see Fig. 6) can be defined by assuming equilibrium with a reservoir of the

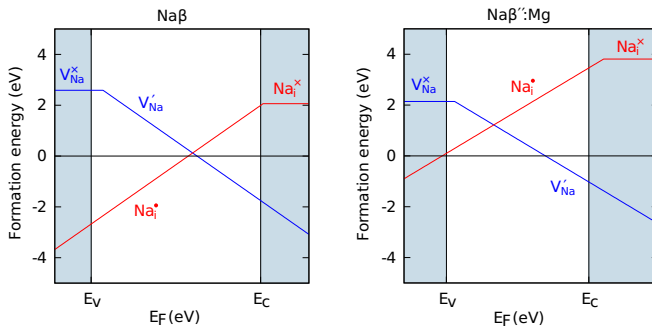


FIG. 6. Vacancy and interstitial formation energies in Na-poor conditions (with chemical potentials defined by Na_2S_4 and S_8 reservoirs). The formation energies for defects in the β alumina phases are shown on the left, and those in the Mg-stabilized β' alumina phases are shown on the right. The band gap values were calculated and can be found in the Appendix (Tables II and III).

sodium polysulfide Na_2S_4 and sulfur, which results in vacancy formation energies that are about 2 eV lower than in Na-rich conditions. In general, battery voltages are of the order of eV, corresponding to the difference in the X chemical potential at the X -poor side and at the X -rich side of the battery.

Finally, we note that the calculated band gap is underestimated as expected using the DFT-PBE functional. Assuming that the defect levels are pinned to the band edges, correcting the band gap could lead to vanishing defect formation energies near midgap.

D. Migration energies

The activation energies for migration of X vacancies and interstitials have been calculated assuming that they are always in their respective charged states ($q = -1$ for V_X' and $q = 1$ for X_i^\bullet). The charged supercell calculations were carried out as detailed in Sec. III C. The activation energies are found by searching the minimum-energy path between two equivalent positions separated by a lattice vector, using the NEB method (see Methods section), and taking the difference between the energies at the saddle point and at the minimum-energy point. All the migration energies presented here are for mechanisms that allow for long-range diffusion.

1. Vacancy migration

β alumina. Figure 7 shows a hop of the Na vacancy in Na β alumina from one BR site to another, and the corresponding energy profile. The saddle point is at the middle plane equidistant to the initial and final configurations. The migration path is similar for K β alumina. In Li β alumina, the Li vacancy is not trigonal, due to the original position of the Li atoms closer to the bridge oxygen atoms. The Li vacancy migration involves a jump of one of its Li neighbors to the bridge oxygen atom near the vacancy, breaking two Li-O bonds, but still requires a lower activation energy than in the cases of Na or K. The respective activation energies can be found in Table I.

Mg-stabilized β'' aluminas. In the β'' conduction region, the X atoms form a honeycomb lattice and are $1/\sqrt{3}a_0$

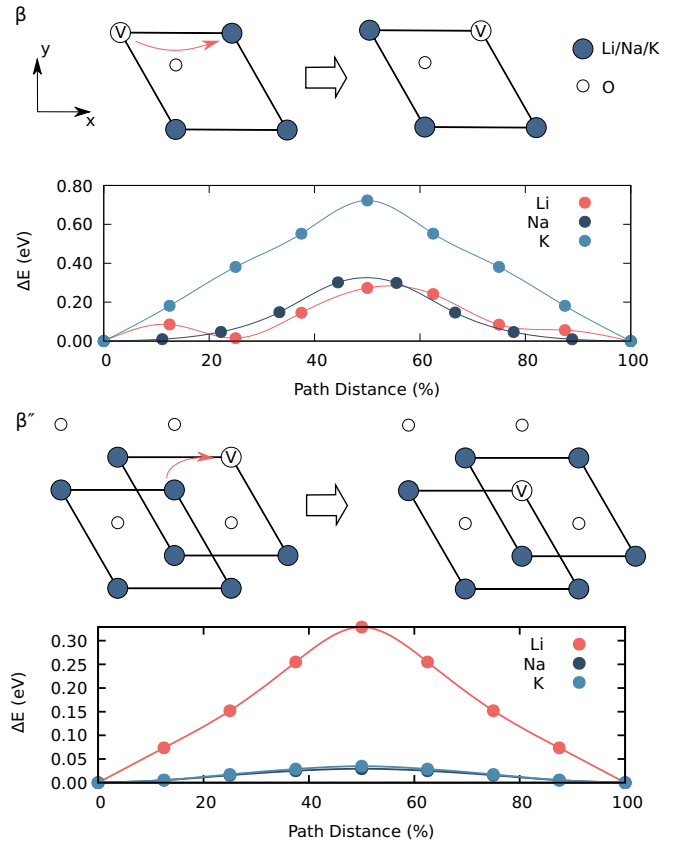


FIG. 7. Schematic of the vacancy migration pathways in β aluminas (top) and Mg-stabilized β'' aluminas (bottom) along with their respective energy profiles.

apart, closer than in β alumina. The migration energy for the vacancy hop is 0.33, 0.03, and 0.03 eV for Li, Na, and K, respectively (Table I).

We have also investigated the two-atom correlated process where one atom jumps into the neighboring vacancy and its neighbor jumps to the site just vacated (Fig. 7) has an activation energy of just 0.32, 0.08, and 0.02 for Li, Na, and K, respectively. The concerted movement allows two atoms to move with approximately the same energy as one atom for Li and K. It is possible that concerted migration involving more atoms is also energetically favored, but we could not investigate it due to the size limit imposed by the supercell dimensions. The supercell dimensions also affect the extended X atomic displacements due to the vacancy, and thus the small migration energies obtained for Na and K are already close to the uncertainty of our calculations.

Since the β'' aluminas are often alkali-metal deficient, these migration energies can be considered lower bounds for the activation energy for the conductivity, which have been experimentally determined to be 0.30, 0.03 (at high temperature) and 0.15 eV in Li, Na, and K β'' aluminas, respectively [10].

The exceptionally low activation energy found for V_K' in K β'' : Mg corroborates the experimental observation of room-temperature ionic conductivity of K β'' phase [12] being 2000 times higher than K β and 10 times higher than that of Na β'' alumina.

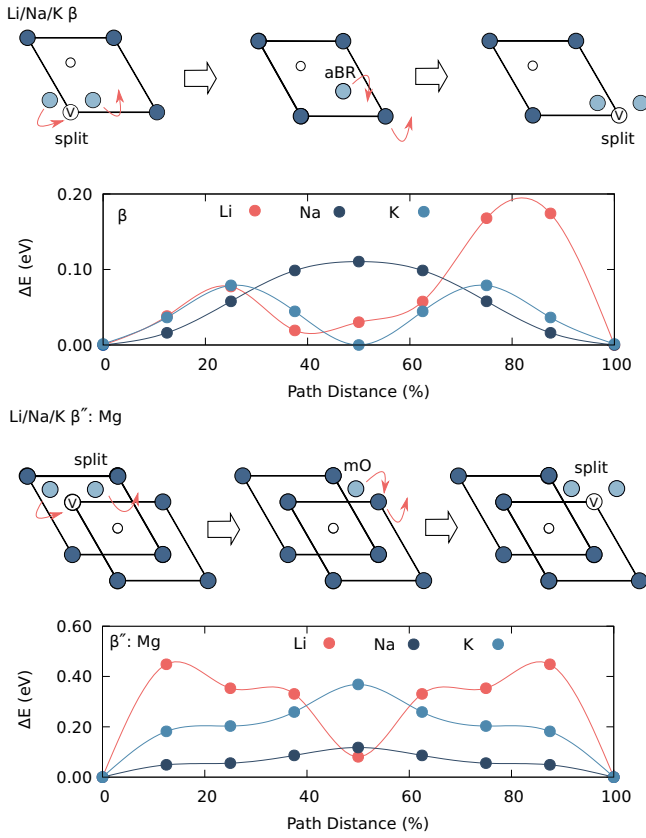


FIG. 8. Schematic representation of Li, Na, and K interstitial migration in the respective β alumina (top) and Mg-stabilized β'' alumina (bottom), alongside the calculated energy profile. Different from all other X self-interstitials which have the orientation represented in the figure, the Li split-interstitial in Li β alumina is oriented approximately along [110] but follows a similar migration path. The migration path distance is from a split-interstitial position to a neighboring split-interstitial position (at 0% and 100%), through the aBR site in the case of β alumina, or through the mO site in the case of Mg-stabilized β'' alumina. For orientation and color code, please refer to Fig. 4.

2. Interstitial migration

Since the X interstitials in all β and β'' alumina materials considered are split-interstitials, their migration necessarily involves at least two atom jumps.

β aluminas. Figure 8 shows schematically the migration of a split-interstitial in β alumina along one of the principal in-plane crystal directions. The saddle point is an interstitial at the aBR site, a configuration at the mirror plane equidistant to the initial and final configurations. While one of the split-interstitial atoms hops to the vacant site, the other one hops through the aBR site, knocking on the next X atom to create another split-interstitial one lattice spacing away.

The energy profile shows a monotonic increase from the split-interstitial to the aBR site for Na but not for Li and K (Fig. 8).

In the case of the Li β alumina, the nonmonotonic behavior is due to the out-of-plane movement of the migrating Li atoms, which approach the neighboring oxygen atoms of the spinel layers at each point of the trajectory. The case of Na β

alumina can be understood taking into account the contribution of the Coulomb potential energy, which is dominant in the case of Na [26]. The $\text{Na}^+ \text{-Na}^+$ repulsive Coulomb potential energy is highest at the aBR site, resulting in a saddle point of the energy surface at this point. Sharing the BR site in a split-interstitial configuration is energetically more favorable. K has a higher ionic radius of 1.463 Å [26]. The split-interstitial thus has a 3.47 Å distance between the K interstitials, whereas the distance between the aBR K interstitial and its neighbors is 3.45 Å. The energy of the two configurations is therefore nearly degenerate.

The migration energies can be found in Table I. The interstitial migration energies are lower than the vacancy migration energies for all β alumina. Coupled to the low- X interstitial formation energy this indicates that an interstitial-mediated mechanism is the dominant process of ionic conduction. The activation energies 0.17, 0.09, and 0.08 eV for Li, Na, and K, respectively, can be considered lower bounds for the activation energy for conduction, which has been experimentally measured to be 0.24, 0.15, and 0.28 eV, respectively [10].

Mg-stabilized β'' aluminas. As for Mg-stabilized β'' aluminas, the X interstitials migrate through the available mO sites (Fig. 8). One of the atoms in the split interstitial migrates to the vacant site while repelling the other, which knocks off one of its nearest neighbors into an available mO site. This mO interstitial then can relax to a split-interstitial centered on another lattice site. The process is not always on the plane, as the X atoms in the two BR or aBR sublattices are staggered, and more packed than in the β aluminas. The respective activation energies for this process are 0.45, 0.12, and 0.37 eV for Li, Na, and K, respectively. All these are higher than the respective vacancy migration energies (Table I). The energy profiles for the interstitial migration in the three β'' materials can be found in Fig. 8.

IV. DISCUSSION

A. Comparison to experimental activation energies

We now compare the migration energies that we have obtained to the activation energies that have been determined from conductivity experiments. As commented in the introduction, in β and β'' aluminas, the number of X cations per conduction plane per unit cell is between one (the ideal value for β alumina) and two (the ideal value for β'') alumina. Thus, cation interstitial and vacancy defects are already present from growth and the contribution of the defect formation energy will be neglected.

Li β and β'' aluminas. Li β and β'' aluminas are usually prepared from the corresponding Na crystals by ion exchange [13], the activation energy for conduction was determined to be 0.24 eV for complete ion exchange. This agrees well with our calculated 0.17 eV for the migration energy of the Li interstitial. The slightly higher value of 0.27 eV reported for single crystals [50] may be due to mixed alkali effect, as the samples had 93% Li. The temperature dependence has only been reported up to 500 K and it is not clear whether there will be a transition to a high-temperature regime similar to what is observed in the mixed Li-Na β aluminas [13]. There is little information for Li β'' aluminas apart from that

collected by Bates [10], which gives an activation of 0.30 eV in reasonable agreement with our estimate for the Li vacancy, of 0.32–0.33 eV. We have only considered correlated diffusion with jumps of up to two atoms (second-nearest-neighbor displacement). Possibly, the migration energy of the vacancy can be even lower if more than two atoms are allowed to jump simultaneously.

Na β alumina. This is the most well-studied system, and the activation energy measured in single-crystals is 0.16 eV [10], slightly above our estimate of 0.09 eV for the Na interstitial migration. This indicates that there may be room for optimization. Factors increasing the activation energy may include the presence of water and oxygen interstitials in the conduction plane. The conduction is Arrhenian with a single activation energy from 300 to 600 K.

Na β'' alumina. The temperature dependence of the conductivity of Na β'' aluminas is not Arrhenian. The activation energy ranges from 0.03 eV at high temperature up to 0.3 eV at low temperature. The low temperature regime has been explained as resulting from vacancy ordering or interaction with compensating defects [61,69]. The lower bound is in agreement with our estimate for the Na vacancy migration.

K β and β'' . For K β alumina, we found only the measurements of Ref. [67]. There is a range of variation of the activation energy from 0.28 to 0.56 eV depending on the growth method, curiously with higher activation energy found for the most-ordered material. All samples had a cation excess of 0.16–0.38 per conduction plane per unit cell. All the measured activation energies are much higher than our calculated migration energy for the K interstitial (0.08 eV), indicating that there is room for optimization. In the case of the K β'' aluminas, the temperature dependence of the conductivity is non-Arrhenian, with activation energies ranging from 0.09 eV at high temperature to 0.186 eV at low temperature, similar to the case of the Na β'' alumina [10,16,25]. Both values are higher than the calculated migration energy for the K vacancy. The feasibility of such small migration energy will be further discussed in the next section.

B. The small V_X migration energy in β'' aluminas

The V_X migration energies in Na and K β'' aluminas are the smallest among all the systems considered. This result is to be expected in the basis of earlier works investigating the potential-energy surface in the conduction regions based on classical potentials [26,33]. The total potential energy of an ion along the migration path (in this case, from one of the X sites neighboring V_X into V_X) results from the sum of the contributions of Wang *et al.* [26]:

- (1) the long-range potential energy, which is approximately the same for all ions with the same effective charge;
- (2) the short-range repulsion, which depends on the ionic radii; the radii of K and Na are in this case larger than that of Li;
- (3) the polarization energy, which depends on the polarizability; the polarizability is the largest for the ions with more electrons.

The Coulomb potential and short-range repulsion partially cancel each other in Na β'' alumina resulting in a potential-energy barrier of about 0.2 eV for motion of a single atom in

a (hypothetical) empty conduction plane [33]. When the other Na ions are present in the plane, there is additional Na-Na ion repulsion. Additionally, the concerted movement of the X atoms contributes to lowering the energy barrier. The resulting activation energy for correlated diffusion of the vacancy was estimated to be only 0.02 eV or nearly free [26], in excellent agreement with our calculation.

Since K has a slightly larger ionic radius, correlated movement in plane is expected to be even more important than in the case of Na. To assess the contribution of the correlated motion of K ions to lowering the migration barrier, we have calculated the energy barrier for migration of a single K^+ vacancy in K β'' , with a single moving K^+ ion, and keeping all other atoms fixed; this was found to be 0.52 eV, much larger than the barrier 0.02–0.03 eV calculated with all the K ions mobile. This agrees with the predictions of Wang *et al.*, supporting the idea that the correlated motion is essential for the low migration energy of X vacancies in Na and K β'' aluminas.

Finally, a factor that influences the accuracy of the calculations is the use of a semilocal functional for the DFT calculation. The exchange-functional used in the calculations affects the lattice constants, which in turn can affect the relative energies of different structures. A study of molecular adsorption on surfaces found that the results of the PBE functional are usually a good compromise, yielding results similar to those obtained with a hybrid functional [70]. Since the defects that we study here are charged for almost nearly every Fermi-level position across the band gap, changes in structure associated with spurious changes in the charge state are not expected. However, the migration energies of defects can still be underestimated as a result of the band gap underestimation, as illustrated by the case of the copper interstitial defect in silicon [71] which, similar to the X_i in β and β'' aluminas is charged for any Fermi-level position.

C. Lower bound for the activation energies

There are some experimental observations in Na and K β'' aluminas that may be relevant to understanding how low, in practice, can the activation energy in these materials be.

Raman-scattering experiments at 15 K in Na and K β'' aluminas find very low cation vibrations at 33 and 73 cm^{-1} which indicate a flat potential-energy surface [27].

However, below room temperature, it is believed the interaction of vacancies with Mg and with other vacancies becomes dominant, leading to higher activation energies of the conductivity of 0.18 eV both in Na and K β'' aluminas [25]. Vacancy ordering has been observed at low temperatures using diffuse x-ray scattering [46]. At room temperature, the activation energy of the conductivity is 0.10 and 0.09 eV in Na and K β'' aluminas, respectively [25]. This is still higher than our estimates. At higher temperatures up to 300°C, the activation energy can reach 0.03 eV for Na β'' alumina [10].

Additionally, it should be taken into account that K β'' aluminas are usually prepared starting from Na β'' aluminas by ion exchange. Incomplete ion exchange can lead to higher activation energies due to entropy- the “mixed alkali effect” [72].

Lastly, water intercalation in β'' aluminas [10] may influence the conduction mechanism.

V. CONCLUSION

We have carried out DFT calculations of the structure, formation energy and migration of intrinsic defects in β and β'' aluminas of Li, Na, and K. We have confirmed that both alkali-metal self-interstitials and vacancies in the conduction plane can carry charge almost for the whole range of Fermi-level energies potentially available.

Alkali-metal self-interstitials have low or even negative formation energy in β aluminas in alkali-metal-rich conditions, and this is consistent with Na excess reported experimentally [67]. The X_i activation energies for migration are slightly lower than the experimental activation energies, which could be due to the formation energy contribution or to crystal imperfection.

The formation energies of alkali-metal vacancies in β'' aluminas are positive over most of the DFT band gap even in the case of Na-poor Na β'' alumina. However, such defects can possibly be present due to high-temperature processing. Similarly, the structure can be made less Li, Na, K stuffed (but stoichiometric) by adding less Mg_{Al} .

In the β aluminas, alkali-metal vacancy migration energies increase with increasing ionic radius, but the alkali-metal interstitial migration energy decreases with ionic radius, which is somewhat counterintuitive. In the β'' aluminas, the vacancy migration energies for Na and K are about one order of magnitude lower than for Li. The atomic radii of Na and K are just ideal to move in a snug fit in the interlayer spacing when it is close to maximum packing.

The vacancy migration energy 0.03 eV that we have obtained for Na β'' alumina is closer to the experimental value for the high-temperature regime. It has been suggested that the higher activation energy at low temperatures is due to vacancy ordering [61,69]. Recently, it has been proposed that interaction between the vacancies and the Mg_{Al} is at the origin of higher activation energy in the low-temperature regime [35], an explanation that reconciles the experimental interpretation with the results of our calculations. Comparing the energy of the correlated two-atom process with the one-atom process for vacancy migration in β'' aluminas, we found that the energy of the two is nearly the same in the cases of Li and K, indicating that the uphill movement of one atom on its potential-energy surface is correlated with the downhill movement of the other atom [73]. Such processes involving two or more atoms may contribute significantly to diffusion. The Haven ratio, which is defined simply as the ratio of the tracer diffusion coefficient to a diffusion coefficient obtained from the ionic conductivity via the classical Nernst-Einstein equation, has been employed as a measure of the ionic correlation [74]. Unfortunately, there is a lack of measurements of the Haven ratio in β'' aluminas.

The calculated activation energy for V'_K in K β'' alumina is found to be only about 20 meV, suggesting that this material can present nearly ideal ion conduction if the amount of K is carefully controlled. The smaller energy barrier found in K β'' alumina is due to its optimal ionic radius together with lower affinity of K for O when comparing with

TABLE IV. Cohesive energies (eV) of lithium, sodium and potassium oxides.

Compound	Cohesive energy (eV)
Li ₂ O	-5.93
Na ₂ O	-4.02
K ₂ O	-3.47

the other alkali metals (see Table IV). We therefore believe that K β'' alumina deserves further attention as an ionic conductor.

ACKNOWLEDGMENTS

This research project is supported by the Ministry of Education, Singapore, under its Research Centre of Excellence award to the Institute for Functional Intelligent Materials, National University of Singapore (I-FIM, project No. EDUNC-33-18-279-V12). This work used computational resources of the supercomputer Fugaku provided by RIKEN (Project ID: hp230186); the Centre of Advanced 2D Materials (CA2DM), funded by the National Research Foundation, Prime Ministers Office, Singapore; and the Singapore National Supercomputing Centre (NSCC).

APPENDIX A: CALCULATED LATTICE PARAMETERS AND BAND STRUCTURES

The calculated lattice parameters a , b , and c are given in Tables II and III. For hexagonal systems, \mathbf{a} and \mathbf{c} are aligned with \hat{x} and \hat{z} directions, respectively. The respective crystallographic information files (CIF) are given as Supplemental Material [54].

For direct comparison, we represent the orthorhombic structure of the Li β phase in the same orientation, with \mathbf{a} and \mathbf{c} lattice vectors aligned with the \hat{x} and \hat{z} directions respectively. The \mathbf{b} vector is perpendicular to \mathbf{c} and makes an angle of 120° with \mathbf{a} . For a standard crystallographic representation, refer to the CIF file in Supplemental Material [54].

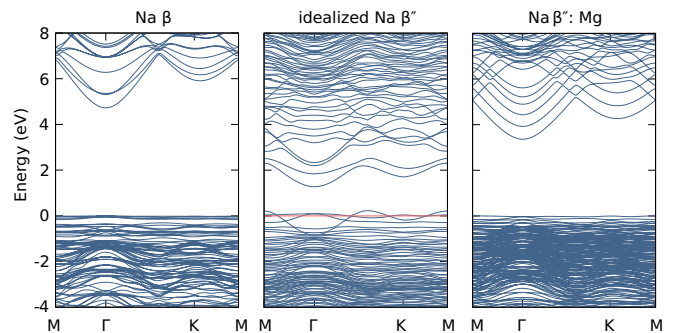


FIG. 9. Electronic band structures of Na β , idealized Na β'' and Mg-stabilized Na β'' ($x = 1$) phases. For Na β alumina and Mg-stabilized Na β'' alumina, the valence-band maxima was set to zero. For the idealized Na β'' alumina, the Fermi level is set to zero.

Supplemental Material also includes additional projections of the structures.

The electronic band structures and band gaps (see Fig. 9) were obtained using DFT in the PBE approximation as detailed in Sec. II.

APPENDIX B: COHESIVE ENERGIES OF ALKALI-METAL OXIDES

Cohesive (atomization) energies of the ground-state oxides are given in Table IV.

- [1] J. G. Kim, B. Son, S. Mukherjee, N. Schuppert, A. Bates, O. Kwon, M. J. Choi, H. Y. Chung, and S. Park, A review of lithium and non-lithium based solid state batteries, *J. Power Sources* **282**, 299 (2015).
- [2] C. Li, Z.-y. Wang, Z.-j. He, Y.-j. Li, J. Mao, K.-h. Dai, C. Yan, and J.-c. Zheng, An advance review of solid-state battery: Challenges, progress and prospects, *Sustain. Mater. Technol.* **29**, e00297 (2021).
- [3] J. Janek and W. G. Zeier, Challenges in speeding up solid-state battery development, *Nat. Energy* **8**, 230 (2023).
- [4] H. Zhang, C. Li, M. Piszcz, E. Coya, T. Rojo, L. M. Rodriguez-Martinez, M. Armand, and Z. Zhou, Single lithium-ion conducting solid polymer electrolytes: Advances and perspectives, *Chem. Soc. Rev.* **46**, 797 (2017).
- [5] N. J. Dudney, W. C. West, and J. Nanda, *Handbook of Solid State Batteries*, Vol. 6 (World Scientific, Singapore, 2015).
- [6] L. Kong, L. Wang, J. Zhu, J. Bian, W. Xia, R. Zhao, H. Lin, and Y. Zhao, Configuring solid-state batteries to power electric vehicles: A deliberation on technology, chemistry and energy, *Chem. Commun.* **57**, 12587 (2021).
- [7] M. P. Fertig, K. Skadell, M. Schulz, C. Dirksen, P. Adelhelm, and M. Stelter, From high- to low-temperature: the revival of sodium-beta alumina for sodium solid-state batteries, *Chem. Eur. J.* **5**, e202100131 (2022).
- [8] X. Lu, J. P. Lemmon, V. Sprenkle, and Z. Yang, Sodium-beta alumina batteries: Status and challenges, *JOM* **62**, 31 (2010).
- [9] L. O. Valøen and J. N. Reimers, Transport properties of LiPF₆-based Li-ion battery electrolytes, *J. Electrochem. Soc.* **152**, A882 (2005).
- [10] J. B. Bates, J. Wang, and N. J. Dudney, Solid electrolytes: The beta aluminas, *Phys. Today* **35**(7), 46 (1982).
- [11] J. P. Lemmon and K. D. Meinhardt, Planar high density sodium battery, US Patent No. 9,276,294 (1 March 2016).
- [12] J. Briant and G. Farrington, Ionic conductivity in Na⁺, K⁺, and Ag⁺ β''-alumina, *J. Solid State Chem.* **33**, 385 (1980).
- [13] J. Briant and G. Farrington, Ionic conductivity in lithium and lithium-sodium beta alumina, *J. Electrochem. Soc.* **128**, 1830 (1981).
- [14] T. Tsurumi, G. Singh, and P. S. Nicholson, The mixed alkali effect in (Na⁺ - K⁺) β''-alumina, *Solid State Ionics* **22**, 225 (1987).
- [15] G. M. Crosbie and G. J. Tennenhouse, Potassium beta''-alumina membranes, *J. Am. Ceram. Soc.* **65**, 187 (1982).
- [16] R. Williams, B. Jeffries-Nakamura, M. Underwood, M. Ryan, D. O'Connor, and S. Kikkert, High temperature conductivity of potassium-β''-alumina, *Solid State Ionics* **53-56**, 806 (1992).
- [17] X. Lu, M. E. Bowden, V. L. Sprenkle, and J. Liu, A low cost, high energy density, and long cycle life potassium-sulfur battery for grid-scale energy storage, *Adv. Mater.* **27**, 5915 (2015).
- [18] A. C. Baclig, G. McConohy, A. Poletayev, A. Michelson, N. Kong, J.-H. Lee, W. C. Chueh, and J. Rugolo, High-voltage, room-temperature liquid metal flow battery enabled by Na-K[K-β''-alumina stability, *Joule* **2**, 1287 (2018).
- [19] K. Schierle-Arndt, G. Huber, S. N. Heavens, J. S. Blackburn, and I. W. Jones, Solid polycrystalline potassium ion conductor having a β''-Al₂O₃ structure, its production and the preparation of potassium metal using this potassium ion conductor, US Patent No. 8,551,319 (19 February 2013).
- [20] Y. Xu, T. Ding, D. Sun, X. Ji, and X. Zhou, Recent advances in electrolytes for potassium-ion batteries, *Adv. Funct. Mater.* **33**, 2211290 (2023).
- [21] A. Anderson, The low-energy excitation spectra of Li, Na, K, and Ag beta-alumina, in *Proceedings of the International Conference on Fast Ion Transport in Solids Lake Geneva, Wis*, edited by P. Vashishta, J. N. Mundy, and G. K. Shenoy (North Holland, 1979), p. 255.
- [22] G. Collin, J. P. Boilot, P. Colomban, and R. Comes, Host lattices and superionic properties in β- and β''-alumina. I. Structures and local correlations, *Phys. Rev. B* **34**, 5838 (1986).
- [23] G. Collin, J.-P. Boilot, and R. Comes, Host lattices and superionic properties in β- and β''-alumina. II. Homogeneity ranges and conductivities, *Phys. Rev. B* **34**, 5850 (1986).
- [24] G. Collin, P. Colomban, J. P. Boilot, and R. Comes, X-ray diffuse scattering study of β-alumina B-Mg²⁺ substituted β and β'' alumina, in *Proceedings of the International Conference on Fast Ion Transport in Solids Lake Geneva, Wis*, edited by P. Vashishta, J. N. Mundy, and G. K. Shenoy (North Holland, 1979), p. 309.
- [25] G. C. Farrington and J. L. Briant, Fast ionic transport in solids: Crystalline solids with liquid-like ionic conductivities are revolutionizing solid-state electrochemistry, *Science* **204**, 1371 (1979).
- [26] J. Wang, M. Gaffari, and S.-i. Choi, On the ionic conduction in β-alumina: Potential energy curves and conduction mechanism, *J. Chem. Phys.* **63**, 772 (1975).
- [27] J. Bates, T. Kaneda, W. Brundage, J. Wang, and H. Engstrom, Raman scattering from mobile cations in sodium, potassium and silver beta-aluminas, *Solid State Commun.* **32**, 261 (1979).
- [28] H. Näfe, Relationship between the sodium oxide activity of ceramic (Na-β + β'')-alumina and the sodium activity in the ambience of the material, *Int. J. Mater. Res.* **94**, 962 (2022).
- [29] D. Wolf, On the mechanism of diffusion in sodium beta alumina, *J. Phys. Chem. Solids* **40**, 757 (1979).
- [30] W. L. Roth, F. Reidinger, and S. LaPlaca, Studies of stabilization and transport mechanisms in β and β'' alumina by neutron diffraction, in *Superionic Conductors*, edited by G. D. Mahan and W. L. Roth (Springer, Boston, MA, 1976), pp. 223–241.
- [31] S. W. De Leeuw and J. W. Perram, Motion of charge carrying ions in sodium β-alumina, in *Proceedings of the International Conference on Fast Ion Transport in Solids Lake Geneva, Wis*, edited by P. Vashishta, J. N. Mundy, and G. K. Shenoy (North Holland, 1979), pp. 345–348.

- [32] M. S. Whittingham and R. A. Huggins, Transport properties of silver beta alumina, *J. Electrochem. Soc.* **118**, 1 (1971).
- [33] J. Wang, J. Bates, N. Dudney, and H. Engstrom, Study of β - and β'' -aluminas by means of potential energy calculations, *Solid State Ionics* **5**, 35 (1981).
- [34] B. Hafskjold and X. Li, Molecular dynamics simulations of the Mg^{2+} -stabilized Na^+ -beta''-alumina, *J. Phys.: Condens. Matter* **7**, 2949 (1995).
- [35] A. D. Poletayev, J. A. Dawson, M. S. Islam, and A. M. Lindenberg, Defect-driven anomalous transport in fast-ion conducting solid electrolytes, *Nat. Mater.* **21**, 1066 (2022).
- [36] P. Giannozzi, S. Baroni, N. Bonini, M. Calandra, R. Car, C. Cavazzoni, D. Ceresoli, G. L. Chiarotti, M. Cococcioni, I. Dabo, A. Dal Corso, S. Fabris, G. Fratesi, S. de Gironcoli, R. Gebauer, U. Gerstmann, C. Gougoussis, A. Kokalj, M. Lazzeri, L. Martin-Samos *et al.*, Quantum espresso: A modular and open-source software project for quantum simulations of materials, *J. Phys.: Condens. Matter* **21**, 395502 (2009)..
- [37] J. P. Perdew, K. Burke, and M. Ernzerhof, Generalized gradient approximation made simple, *Phys. Rev. Lett.* **77**, 3865 (1996).
- [38] A. M. Rappe, K. M. Rabe, E. Kaxiras, and J. D. Joannopoulos, Optimized pseudopotentials, *Phys. Rev. B* **41**, 1227(R) (1990).
- [39] H. J. Monkhorst and J. D. Pack, Special points for Brillouin-zone integrations, *Phys. Rev. B* **13**, 5188 (1976).
- [40] R. Fletcher, *Practical Methods of Optimization* (John Wiley & Sons, New York, 2000).
- [41] J. Hannes, M. Greg, and W. J. Karsten, Nudged elastic band method for finding minimum energy paths of transitions, *Classical and Quantum Dynamics in Condensed Phase Simulations* (World Scientific, Singapore, 1998), Chap. 16, pp. 385–404.
- [42] G. Henkelman, G. Jóhannesson, and H. Jónsson, Methods for finding saddle points and minimum energy paths, in *Theoretical Methods in Condensed Phase Chemistry*, edited by S. D. Schwartz (Springer, Dordrecht, 2002), pp. 269–302.
- [43] C. Beevers and S. Brohult, The formula of “ β alumina,” $\text{Na}_2\text{O} \cdot 11\text{Al}_2\text{O}_3$, *Z. Krist., Cryst. Mater.* **95**, 472 (1936).
- [44] C. Beevers and M. A. Ross, The crystal structure of “beta alumina” $\text{Na}_2\text{O} \cdot 11\text{Al}_2\text{O}_3$, *Z. Krist., Cryst. Mater.* **97**, 59 (1937).
- [45] A. Ray and E. Subbarao, Synthesis of sodium β and β'' alumina, *Mater. Res. Bull.* **10**, 583 (1975).
- [46] J. P. Boilot, G. Collin, P. Colomban, and R. Comes, X-ray-scattering study of the fast-ion conductor β'' -alumina, *Phys. Rev. B* **22**, 5912 (1980).
- [47] J. Kummer, β -alumina electrolytes, *Prog. Solid State Chem.* **7**, 141 (1972).
- [48] T. Kaneda, J. Bates, and J. Wang, Raman scattering from $^6\text{Li}^+$ and $^7\text{Li}^+$ ions in lithium beta-alumina, *Solid State Commun.* **28**, 469 (1978).
- [49] M. Villa, J. L. Bjorkstam, G. Mariotto, A. Fontana, and E. Cazzanelli, Lithium ion distribution and motion in β -alumina: An NMR and Raman investigation, *J. Chem. Phys.* **76**, 2804 (1982).
- [50] M. T. Chowdhury, R. Takekawa, Y. Iwai, N. Kuwata, and J. Kawamura, The study of the lithium ion motion in β -alumina single crystal by NMR spectroscopy, *Solid State Ionics* **262**, 482 (2014).
- [51] K. Edström, T. Gustafsson, J. O. Thomas, and G. C. Farrington, Li^+/Na^+ β -alumina: A combined single-crystal neutron and X-ray diffraction study, *Acta Crystallogr., Sect. B: Struct. Sci.* **53**, 631 (1997).
- [52] B. Tofield and G. Farrington, Structure of lithium–sodium β -alumina by powder neutron diffraction, *Nature (London)* **278**, 438 (1979).
- [53] J. Jorgensen, F. Rotella, and W. Roth, Conduction plane and structure of Li-stabilized Na^+ β'' -alumina: A powder neutron diffraction study, *Solid State Ionics* **5**, 143 (1981).
- [54] See Supplemental Material at <http://link.aps.org/supplemental/10.1103/PhysRevB.109.134105> for crystallographic information files; orthographic projections; charge corrections; Mg_{Al} in Mg-doped β'' and NEB trajectories, which also contains Ref. [76].
- [55] K. Edström, Potassium β'' -aluminogallate, *Acta Crystallogr., Sect. C: Cryst. Struct. Commun.* **55**, 1384 (1999).
- [56] J. Sudworth and A. Tiley, *Sodium Sulphur Battery* (Springer Science & Business Media, New York, 1985), p. 42.
- [57] T. Tsurumi, H. Ikawa, T. Nishimura, K. Urabe, and S. Udagawa, Crystal structure and charge compensation mechanism of β'' -alumina type R^+ -gallate ($R = \text{K}^+, \text{NH}_4^+$), *J. Solid State Chem.* **71**, 154 (1987).
- [58] K. Frase, J. Thomas, A. McGhie, and G. Farrington, Proton transport in β'' -alumina, *J. Solid State Chem.* **62**, 297 (1986).
- [59] P. Wynblatt, A calculation of the formation and migration entropies of surface defects in copper, *Phys. Status Solidi B* **36**, 797 (1969).
- [60] E. Simoen and C. Claeys, Diffusion and solubility of dopants in germanium, in *Germanium-Based Technologies*, edited by C. Claeys and E. Simoen (Elsevier, Oxford, 2007), Chap. 3, pp. 67–96.
- [61] H. Engstrom, J. Bates, W. Brundage, and J. Wang, Ionic conductivity of sodium beta''-alumina, *Solid State Ionics* **2**, 265 (1981).
- [62] R. De Souza and G. Harrington, Revisiting point defects in ionic solids and semiconductors, *Nat. Mater.* **22**, 794 (2023).
- [63] T. R. Durrant, Supercell electrostatics of charged defects in periodic density functional theory, Ph.D. thesis, University College London, 2019.
- [64] C. Freysoldt, B. Grabowski, T. Hickel, J. Neugebauer, G. Kresse, A. Janotti, and C. G. Van de Walle, First-principles calculations for point defects in solids, *Rev. Mod. Phys.* **86**, 253 (2014).
- [65] C. Freysoldt, J. Neugebauer, and C. G. Van de Walle, Fully *ab initio* finite-size corrections for charged-defect supercell calculations, *Phys. Rev. Lett.* **102**, 016402 (2009).
- [66] H. R. Gopidi, L. Vashist, and O. I. Malyi, Physics of band-filling correction in defect calculations of solid-state materials, [arXiv:2307.03849](https://arxiv.org/abs/2307.03849).
- [67] S. J. Allen Jr, A. S. Cooper, F. DeRosa, J. P. Remeika, and S. K. Ulasi, Far-infrared absorption and ionic conductivity of Na, Ag, Rb, and K β -alumina, *Phys. Rev. B* **17**, 4031 (1978).
- [68] M. T. Chowdhury, R. Takekawa, Y. Iwai, N. Kuwata, and J. Kawamura, Lithium ion diffusion in Li β -alumina single crystals measured by pulsed field gradient NMR spectroscopy, *J. Chem. Phys.* **140**, 124509 (2014).
- [69] J. Bates, H. Engstrom, J. Wang, B. Larson, N. Dudney, and W. Brundage, Composition, ion-ion correlations and conductivity of beta''-alumina, *Solid State Ionics* **5**, 159 (1981).

- [70] A. Stroppa and G. Kresse, The shortcomings of semi-local and hybrid functionals: What we can learn from surface science studies, *New J. Phys.* **10**, 063020 (2008).
- [71] A. Sharan, Z. Gui, and A. Janotti, Hybrid-functional calculations of the copper impurity in silicon, *Phys. Rev. Appl.* **8**, 024023 (2017).
- [72] P. K. Davies, G. J. Pfeiffer, and S. Canfield, Thermodynamics of mixing in beta alumina-relation to the mixed alkali effect, *Solid State Ionics* **18-19**, 704 (1986).
- [73] X. He, Y. Zhu, and Y. Mo, Origin of fast ion diffusion in super-ionic conductors, *Nat. Commun.* **8**, 15893 (2017).
- [74] G. Murch, The haven ratio in fast ionic conductors, *Solid State Ionics* **7**, 177 (1982).
- [75] T. Takahashi, K. Kuwabara, and H. Ohyanagi, Synthesis of potassium beta-alumina by thermal decomposition of a complex, *J. Appl. Electrochem.* **11**, 77 (1981).
- [76] G. Makov and M. C. Payne, Periodic boundary conditions in *ab initio* calculations, *Phys. Rev. B* **51**, 4014 (1995).